HEFAT2012
9th International Conference on Heat Transfer, Fluid Mechanics and Thermodynamics
16 – 18 July 2012
Malta

Experimental Investigation of a Separation Bubble on a Flat Plate with Semi-circular Leading Edge for different Reynolds Numbers

A. Samson, S. Sarkar* and K. Anand
*Author for correspondence
Department of Mechanical Engineering,
Indian Institute of Technology Kanpur,
Kanpur, 208016,
India,
E-mail: subra@iitk.ac.in

ABSTRACT

The laminar separated layer over a semi-circular leading edge, its transition, turbulent reattachment and downstream development have been investigated in a low-speed wind tunnel. Instantaneous velocity and surface pressure measurements were made along with a planar PIV to visualize flow structures for varying Reynolds number 25000 to 75000 (based on the leading edge diameter). The velocity fluctuations illustrates that the separated shear layer is laminar up to 20% of separation length and then the perturbations are amplified in the second half attributing to breakdown and reattachment. The bubble length is highly susceptible to change in Reynolds number and plays an important role in outer layer activities. It is also evident that the shear layer is inviscidly unstable and the predominant shedding frequency when normalised with respect to the momentum thickness at separation remains almost constant with change in Reynolds number.

Keywords: Leading-edge Separation bubble, Transition, Turbulent flows.

INTRODUCTION

A laminar boundary layer may separate from a surface under the influence of an adverse pressure gradient or because of sudden change in surface curvature. Since a separated shear layer is inviscidly unstable, it usually undergoes a rapid transition and reattaches as turbulent layer. In aerospace applications, a separation bubble occasionally forms on the suction surface of a high cambered low pressure turbine blade or on the leading edge of an aerofoil at high angle of attack. In all these cases, the presence of separation bubble changes the boundary layer characteristics downstream and deteriorates the performance by loss of lift with an increase of drag. It may also act as a source of noise. The schematic of two-dimensional laminar separation bubble found over a leading edge of an aerofoil is shown in Fig 1 following Ref. 1. The recirculation velocity near the separation point is almost stationary and this region is designated as dead air region attributing to a

NOMENCLATURE

Re	[-]	Reynolds Number
U_0	[m/s]	Inlet velocity
U	[m/s]	Local free stream velocity
l	[mm]	Time averaged bubble length
D	[mm]	Leading edge diameter
p	[N/m^2]	Difference between surface pressure and tunnel static pressure
q	[N/m^2]	Dynamic pressure $\left(\frac{1}{2}\rho U_0^2\right)$
C_p	[-]	Coefficient of pressure
$C_p^{'}$	[-]	Pressure recovery coefficient
x	[mm]	Streamwise coordinate
z	[mm]	Wall normal coordinate
u'	[m/s]	r.m.s of Streamwise fluctuating velocity
δ	[mm]	Shear layer thickness
δ^*	[mm]	Displacement thickness
θ	[mm]	Momentum thickness
H	[-]	Shape factor
u_e	[m/s]	Local free-stream velocity
ν	[m^2/s]	Kinematic viscosity
m	[-]	Thwaites parameter
Λ_R	[-]	Horton parameter
$St_{\theta S}$	[-]	Strouhal number based on momentum thickness at separation
K	[1/m]	Wave number
f	[Hz]	Frequency
$Re_{\theta S}$	[-]	Reynolds number based on momentum thickness at separation

Subscripts

max	Maximum
min	Minimum
S	Separation
R	reattachment

constant pressure distribution. A region of strong recirculation velocity is observed near the reattachment with a rapid increase of surface pressure. One important concern regarding the occurrence and behaviour of leading edge separation bubble is that it plays an important role in determining the character of boundary layer, propagation of turbulence and there by characterising the stall condition of an aerofoil. The low *Re* conditions particularly at high cruising altitudes further deteriorates the performance. Thus, it is important to accurately predict the onset of the separation bubble including its transition, reattachment and further development downstream for a wide range of *Re*.

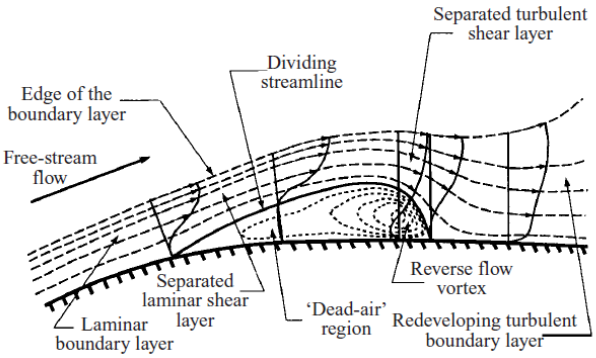

Figure 1 Mean flow structure of a laminar separation bubble.

Extensive studies have been reported illustrating growth of disturbance in a separated layer leading to breakdown. The existence of laminar separation bubble on an aerofoil was first recognized by Jones [2] demonstrating the influence of the bubble on stalling process of aerofoils. The most notable advancement in understanding the bubble structure and behaviour came with the work of Gaster [3]. He demonstrated the instability, breakdown apart from criterion for bubble busting for combinations of pressure distribution and *Re*. Horton [1] proposed a semi empirical model describing the growth and bursting of the bubbles. It should be noted that a laminar separation bubble occasionally forms on aerofoils and stalling is ultimately determined by the bursting, where reattachment may occur far downstream or might not.

Many experimental studies [4-6] demonstrated the development of large-scale flow structures, unsteadiness, vortex shedding and low frequency flapping of separated shear layer resulting in shrinkage and enlargement of reattachment point. The average frequency of vortex shedding measured by several authors [4-6] was about 0.6 to $0.7U_0/l$ and low frequency flapping occurred in the range of 0.12 - $0.2U_0/l$, where U_0 is free stream velocity and l time averaged bubble length.

The instability mechanism of the separated shear layer plays a significant role in breaking down to turbulence followed by its reattachment. Hot wire measurements of Watmuff [7] and PIV/LDA measurements along with Direct Numerical Simulation (DNS) data of Lang et.al and Marxen et al. [8,9] elucidated that instability was initiated through amplification of Tollmien-Schlichting (TS) wave in the upstream of separation and thereafter Kelvin-Helmholtz (K-H) instability sets in forming three-dimensional vortices in the shear layer leading to breakdown and reattachment. Time-resolved PIV measurements of Hain et al. [10] demonstrated the dynamics of laminar separation bubble occurred on an aerofoil for different angle of attack illustrating that K-H instability is the dominant mechanism leading to transition of separated shear layer.

Apart from experiments, there are numerical studies [11,12] that equally contributed in understanding the transition of a separated shear layer. DNS of Spalart and Strelets [13] on a laminar separation bubble formed on a flat plate predicted that transition involves wavering of shear layer and then K-H vortices. However, the DNS of Alam and Sandham [14] on short laminar separation bubble with turbulent reattachment has predicted that shear layer transition occurs via Λ-vortex-induced breakdown leading to turbulent reattachment and relaxes to turbulent profile in far downstream. They have also shown the condition for absolute instability to occur is of the order of 15 - 20% of reverse flow. Recent numerical study of McAuliffe and Yaras [15] on a separation bubble formed over a flat plate suggested that the shear layer undergoes transition through K-H mechanism under low free-stream turbulence (*fst*), whereas, the transition occurs through transient growth or non-modal growth at high *fst*. Yang and Voke [16] carried out a LES over a blunt leading edge demonstrating that the separated shear layer is inviscidly unstable via K-H mechanism and a significant growth of three-dimensional motions occurs at the second half of the bubble with appearance of hairpin vortices leading to breakdown and reattachment. They further indicated that the instantaneous reattachment point moves about 50% of mean reattachment length because of vortex shedding.

Many authors [11,12,16,17] have non-dimensionalised the dominant instability frequency using the momentum thickness and the edge velocity at separation as the characteristic length and velocity scale. Studies of Talan and Hourmouziadis [17] reported $St_{\theta s}$ as 0.010 – 0.014, when transition occurred through K-H mechanism. PIV measurements of McAuliffe and Yaras [18] on an aerofoil for low *Re* reported the value in the range of 0.008 – 0.013. Ripley and Pauley [11], Muti Lin and Pauley [12] have given the value in the range of 0.005 – 0.008. LES of Yang and Voke [16] on a flat plate with semicircular leading edge predicted that frequency lies in the range of 0.005 – 0.011. Extensive studies have been presented in the past to understand the transition of a separation bubble formed over a flat plate, whereas, relatively few attempts [16,19] have been made to elucidate the separated flow characteristics from the leading edge of an aerofoil. It should be noted that the leading-edge separation bubble controls the downstream boundary layer characteristics and stalling behaviour of the aerofoil. The behaviour of the separation bubble also changes with *Re* and *fst*.

In this paper, the characteristics of a laminar separation bubble from semi-circular leading-edge of a flat plate has been documented for a wide range of *Re* from

25000 to 75000 using hot wire and PIV measurements. It has discussed issues regarding shear layer instability, transition, receptivity, growth of perturbations, unsteady vortex shedding, breakdown, reattachment and downstream development of boundary layer, comparing with existing literature and correlations. In brief, the paper illustrates the insight of leading-edge separation bubble, which can also be used for validations.

EXPERIMENTAL DETAILS

A low speed suction type wind tunnel is used to carry out experiments where, the flow enters through 25mm diameter and 162.5mm long flow straightener followed by screens of coarser and finer wire diameter respectively. A two dimensional contraction of 3:1 is designed to dampen the fluctuations and to meet the desired velocity in the test section with a cross section of 324mm ×178mm, 1350mm long and has 0.6^0 divergence over its length to avoid centreline acceleration and to ensure uniform flow in the transverse plane of the tunnel. After the test section, a diffuser is employed to reduce the velocity. A flat plate with semi-circular leading edge diameter *D* of 80mm is placed at the centre of the tunnel which spans the whole width of the tunnel. The model is firmly held in place by fixing it to the side wall of the tunnel. The semi-circle and flat portions are blend tangentially. The length of the flat portion is 10*D* followed by an extended tail of length 1.5*D* that blends with a diameter of 1/4*D*.

Surface static pressure measurements are carried out using electronically scanned pressure sensor (ESP) with a differential pressure range of ± 2500Pa. ESP consists of 32 scanned ports with individual transducers for each port and two additional reference ports for acquisition and calibration. Prior to acquisition each port is individually calibrated by applying known pressure and the calibration coefficient for individual ports are calculated with the calibration data. The calibration coefficient is stored in voltage and then converted to Pascal through a second degree polynomial function. Acquisition is carried out at the rate of 200*Hz* and then the data is acquired through *NI-PXI* system. For all pressure measurements, tunnel static is considered as the reference. Instantaneous velocity measurements are carried out with Hot-wire Anemometry of Dantec Dynamics in constant temperature mode. The sampling frequency during all the measurements was 5k*Hz,* whereas the flow visualizations are carried out using planar PIV. The acquisition time between the frames is calculated based on free-stream velocity and interrogation area, therefore, it differs with Reynolds number.

RESULTS

MEAN FLOW CHARACTERISTICS

The experiments have been carried out for different inlet velocity U_0 = 5 to 14m/s that gives *Re* 25000 to 75000 based on *D*. The surface pressure has been measured from 32 static pressure ports of diameter 0.8mm drilled along the mid-span of the test specimen from the theoretical stagnation point. The streamwise variations of surface pressure have been non-dimensionalised as $C'_p = \left(C_p - C_{p\min}\right) / \left(C_{p\max} - C_{p\min}\right)$ and are

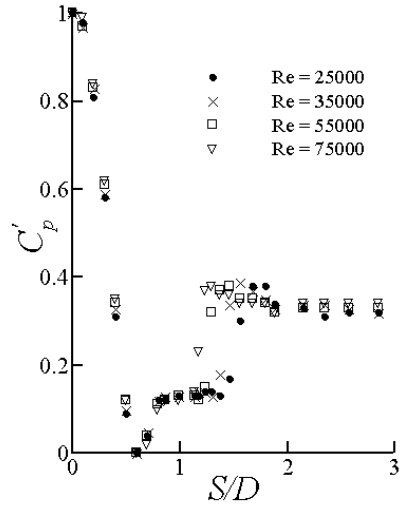

Figure 2 Pressure recovery coefficient along the mid-span from theoretical stagnation point.

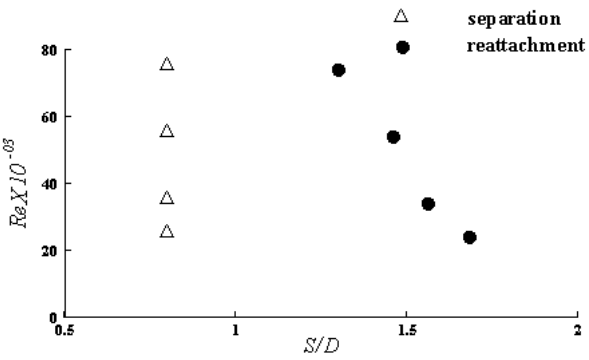

Figure 3 Variation of reattachment length with *Re*.

shown in Fig.2 for different *Re*. The non-dimensionalisation is done following Roshko and Lau [20] and is called pressure recovery coefficient. It is observed that the flow is accelerating along the semi-circular leading-edge attributing to decrease of pressure. The pressure reaches a minimum value after which the flow experiences an adverse pressure gradient followed by a plateau of constant pressure indicating a separated region. At the end of the plateau, the flow experiences an adverse pressure gradient indicating a peak that droops down slowly. The end of reattachment corresponds to the peak in the adverse pressure gradient, whereas, the beginning of constant pressure plateau can be attributed to onset of separation [3,14]. Furthermore, the region of constant pressure can be related to dead air region, whereas, the following strong adverse pressure gradient can be related to the reverse flow vortex as suggested by Horton [1]. It should be noted that the onset of separation and point of reattachment are also verified by Pitot tube measurements along with flow visualizations by PIV. The reattachment point changes significantly with *Re,* whereas, the onset of separation remains almost invariant (being geometry induced separation), illustrating the variation of bubble length with *Re* as described in Fig 3 and Table1.

It should be noted that pressure coefficient $\left(C_p = p/q\right)$ would suffer from instrumental error. The surface pressures as well as the dynamic pressure are measured using pressure scanner, and hence the contribution of uncertainty due to limitations of instrumental precision will be reflected in both. The static error induced in each sensor during calibration is less than ±0.05% of full scale that results in an error in C_p of 0.07%, estimated from $\frac{\Delta C_p}{C_p} = \sqrt{\left[\left(\frac{\Delta p}{p}\right)^2 + \left(\frac{\Delta q}{q}\right)^2\right]}$.

Further, it is inevitable that the instantaneous velocities measured by hotwire will also have errors resulting from calibration against micro-manometer readings. In the present study, an error analysis of measured velocity has been done neglecting uncertainties in atmospheric pressure, density and temperature [33]. Figure 4 illustrates uncertainties in hotwire measurement. The maximum contributions of error are resulted from the reading error of micro-manometer and the effect is more pronounced at low velocity. In the operating range uncertainty is less than 0.3%.

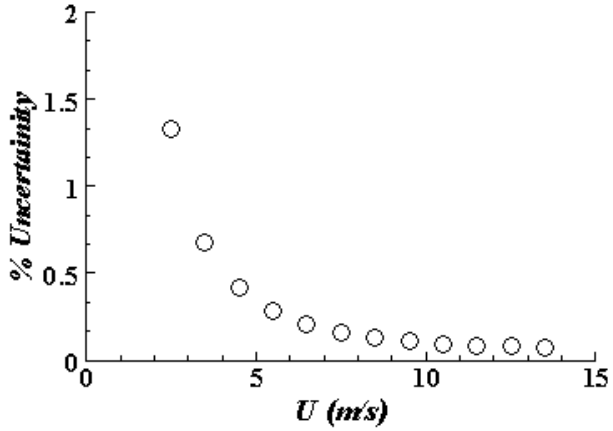

Figure 4 Percentage uncertainty in U and u'.

Figure 5 shows time-averaged streamwise velocity profiles measured using hotwire anemometry for different *Re*. The profiles are normalized by mean bubble length and plotted as a function of *z/l* for six different values of *x/l*. The profiles illustrate flow reversal in the separated region and a velocity deficit that recovers slowly after reattachment. It has been observed that it requires about five bubble lengths to attain an equilibrium profile. The figure also depicts that height and length of the bubble decreases with *Re* and the profiles are not very well scaled with *l* in the separated region.

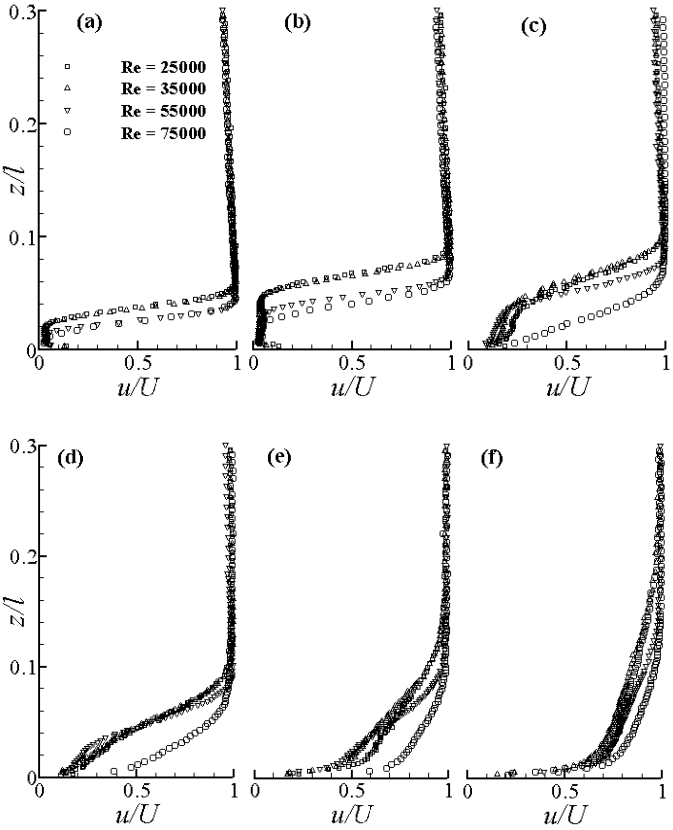

Figure 5 Mean streamwise velocity measured at six different locations from the onset of separation, (a) $x/l = 0.2$ (b) $x/l = 0.5$ (c) $x/l = 0.8$ (d) $x/l = 0.9$ (e) $x/l = 1.2$ and (f) $x/l = 3$.

Figure 6 shows r.m.s fluctuations of stream-wise velocity (u') that begins to increase in the shear layer after separation. During the first half of the bubble the growth rate of u' is slow with appearance of double peak. The outer peak in the shear layer grows rapidly in the second half of the bubble, because of formation of large scale eddies and breakdown. The value of u' becomes maximum near the reattachment. This double peak nature of u' has also been referred by Spalart and Strelets [13]. After reattachment, the near wall turbulence dominates illustrating that

Table 1 Mean bubble characteristics with change in *Re*

Re	l (mm)	h (mm)	θ_s (mm)	l/θ_s	h/θ_s	u_e (m/s)	$St_{\theta s}$
25000	71.5	5	0.207	345.3	24.2	6.02	0.007
35000	62.1	4	0.171	363.2	23.4	8.25	0.008
55000	54.3	3.2	0.125	434.4	25.6	12.73	0.008
75000	37.1	1.5	0.101	368.0	14.9	17.87	0.012

the flow takes several bubble lengths to approach to an equilibrium turbulent layer. What is interesting to note is that the peak of normalised *u'* in the outer layer shifts towards the wall with decrease in magnitude with increase of *Re*, attributing to relatively smaller bubble. Therefore, the bubble length plays an important role in controlling the outer layer activity and thus, augmentation of turbulence.

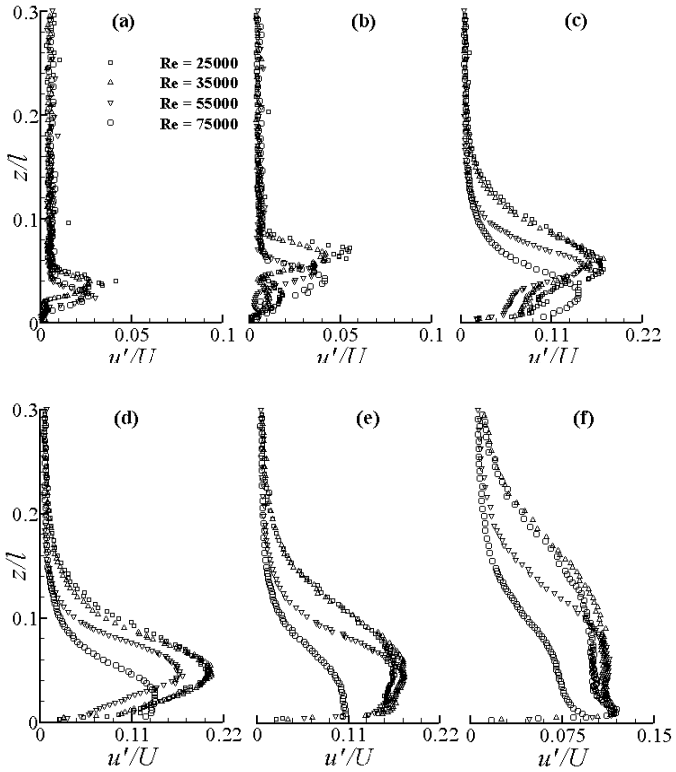

Figure 6 r.m.s of streamwise velocity fluctuation measured at six different locations from the onset of separation, (a) *x/l* = 0.2 (b) *x/l* = 0.5 (c) *x/l* = 0.8 (d) *x/l* = 0.9 (e) *x/l* = 1.2 and (f) *x/l* = 3.

TRANSITION AND DEVELOPMENT OF THREE-DIMENSIONAL MOTIONS

To visualise the internal growth mechanism of shear layer and three-dimensional flow structures, contours of streamwise velocity at three instants are shown in Fig 7 (a) to (c) for *Re* = 35000 from PIV measurements. The flow accelerates over the semi-circular leading edge and it tends to separate from the blend point. The instability of the separated layer occurs because of enhanced receptivity of perturbations. The development of unsteadiness and three-dimensional motions is very significant in the second-half of the bubble with formation of K-H rolls and shedding of large-scale vortices that keep their identity far downstream. This vortex shedding process is attributed to large fluctuations of reattachment point and flapping of shear layer resulting in a maximum change of instantaneous bubble length, which is about 50% of mean bubble length. Yang and Voke [16] observed about 53% change of instantaneous bubble length, where the *Re* was 3450.

Furthermore, the time-averaged streamwise velocity vector along with its contour from PIV data is presented in Fig 7(d). The figure elucidates that onset of separation occurs at the blending point of semi-circular leading-edge and flat plate with reattachment at 60mm, which supports the observation through pressure measurements.

The time traces of streamwise velocity fluctuations for different streamwise locations are shown in Fig 8 and 9, where, measurements are taken at a distance of 1.5mm from the surface. Velocity fluctuations has been normalised with respect to local free stream velocity. For low *Re*, the flow appears to be laminar up to *x/l* = 0.3, after which some pockets of disturbances appear that propagate and grows downstream resulting in random fluctuations, which become maximum near reattachment. For relatively high *Re*, low frequency disturbance appear from the onset of separation that grows in the second-half of the bubble resulting in turbulent fluctuations.

It is seen that the shedding process from a separated shear layer occurs with a range of frequency and energy levels. The shedding frequency is generally normalised based on momentum thickness at separation and local free-stream velocity to get the Strouhal number $St_{\theta S}$ To mention a few, studies on separation bubble over a flat plate reported the values of $St_{\theta S}$ as 0.0068 in Ref. 21 and 0.011 in Ref. 22, whereas, separated layer on an aerofoil gives $St_{\theta S}$ as 0.008-0.013 in Ref. 18. The separation induced by a semi-circular leading-edge produces $St_{\theta S}$ as 0.005 to 0.011 in Ref. 16. In addition, a low frequency flapping of shear layer corresponding to $St_{\theta S}$ = 0.0007-0.001 in Ref 4,16 has also been observed. It was explained by Yang and Voke [16] that during normal vortex shedding, small bubbles are ejected from the tail of a big separation bubble resulting in a slight change in the instantaneous reattachment point. However, the small bubbles may occasionally coalesce and then eject from the separation bubble resulting in a low frequency flapping and large reduction in the reattachment point.

Spectra for instantaneous velocity fluctuations for *Re* = 25000 to 75000 are shown in Fig 10 at different streamwise locations *x/l* = 0.2, 0.6 and 1.0, where, measurements are taken at a distance of 1.5mm from the surface. At *x/l* = 0.2, although excitation of separated layer is apparent by free stream turbulence, the flow appears to be laminar particularly at low *Re*. Further, low frequency oscillations in the range $St_{\theta S}$ = 0.0004-0.0001 are observed here with increase of *Re*, which correspond to low frequency flapping of shear layer reported earlier [4,16]. It should be noted that Ref. 16 reported the value of low frequency flapping as 0.0007-0.001, where the *Re* was 3450. At *x/l* = 0.6 and beyond, the vortex shedding is not periodic, rather there exist a band of frequencies attributing to existence of large, and as well as small-scale eddies. When non-dimensionalised with momentum thickness and local free-stream velocity at the point of separation, the Strouhal number falls in the range 0.004-0.01; 0.002-0.013; 0.001-0.015 and 0.0006-0.015 for *Re* = 25000, 35000, 55000 and 75000 respectively, illustrating that the range of

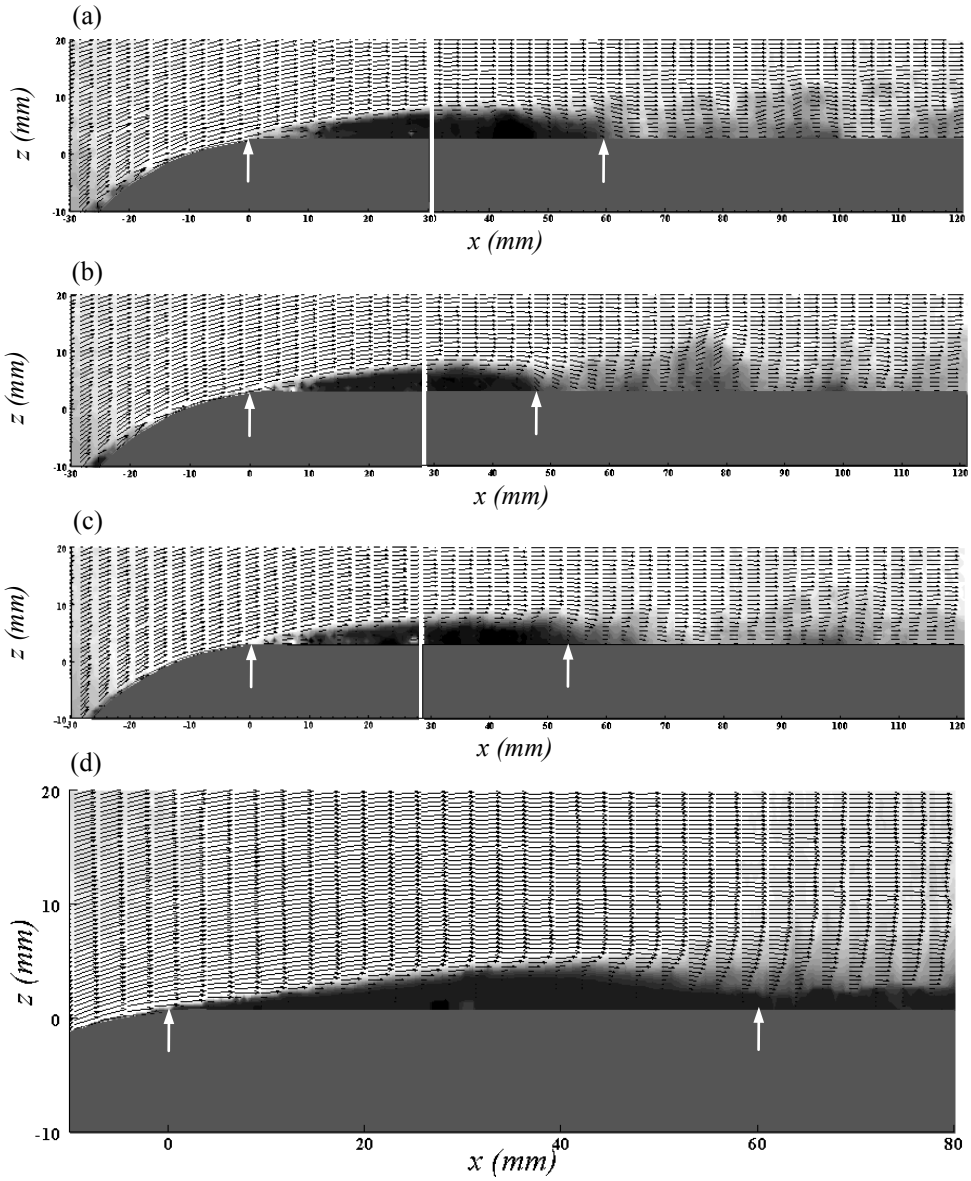

Figure 7 Iso-contours of streamwise velocity along with vectors for *Re* = 35000:(a) - (c) present instantaneous flow field, whereas (d) the averaged bubble. Separation and reattachment points are marked by arrows.

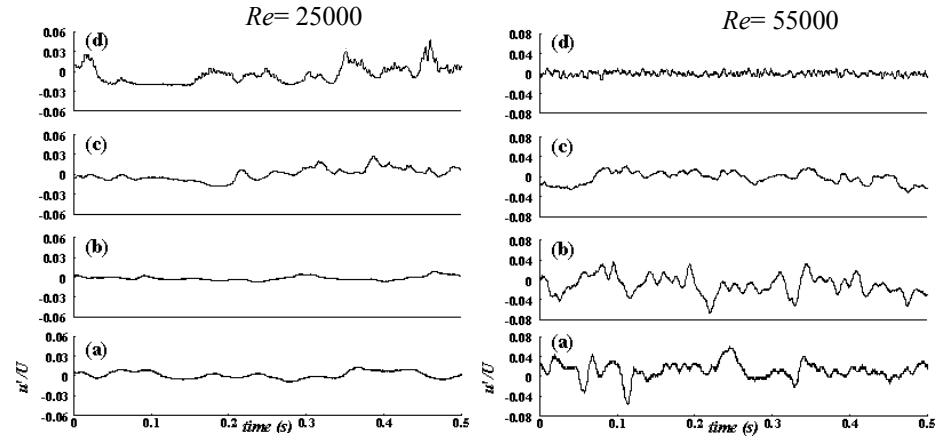

Figure 8 Time series at (a) *x/l* = 0.2, (b) *x/l* = 0.3, (c) *x/l* = 0.4 and (d) *x/l* = 0.5.

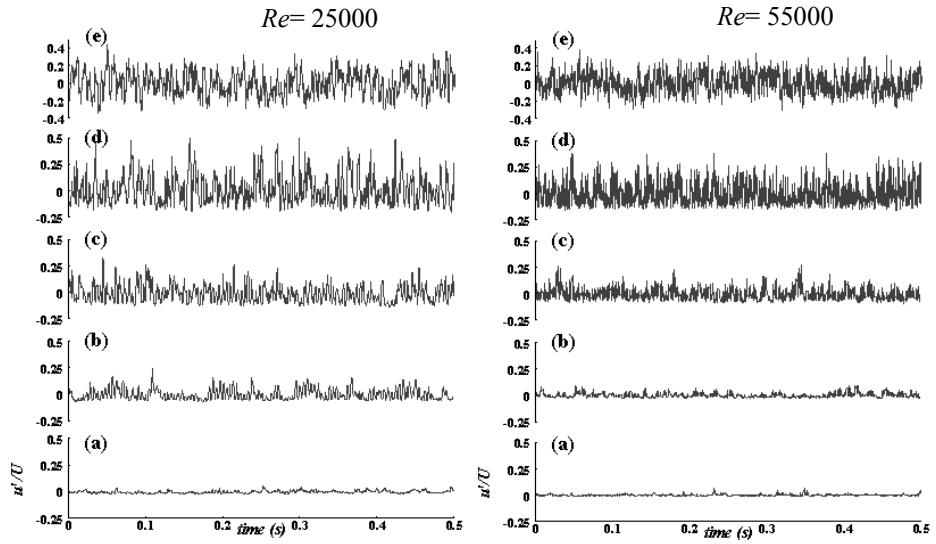

Figure 9 Time series at (a) x/l = 0.6, (b) x/l = 0.7, (c) x/l = 0.8 ,(d) x/l = 0.8 and (e) x/l = 1.2.

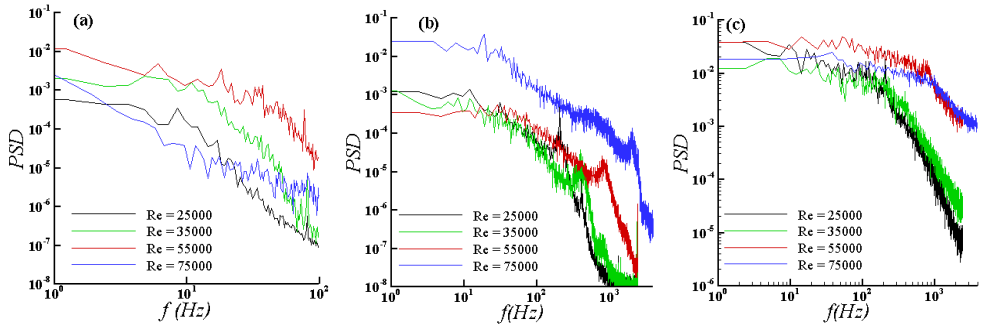

Figure 10 Instantaneous spectra at different stream-wise locations (a) x/l = 0.2, (b) x/l = 0.6 and (c) x/l = 1.

frequencies increases with increase of *Re*, Table 1. Furthermore, the Strouhal number corresponding to the predominant peak shows a very slow variation with *Re* from 0.007 to 0.012. The similar range was observed by others [4, 16,23]. Near reattachment (x/l=1), a band of frequencies appears resembling turbulent spectra with abundant small-scale eddies attributing to breakdown of shear layer.

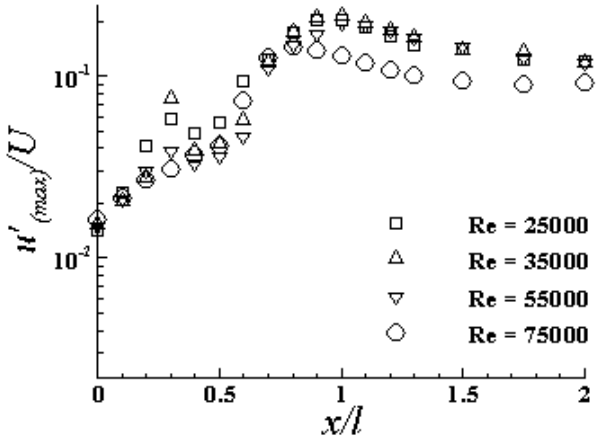

Figure 11 Amplification of disturbances in the stream-wise direction.

Growth of disturbances and development of three-dimensional motions can be well illustrated by the evolution of velocity fluctuations. Fig 11 shows the variation of maximum velocity fluctuation values at different streamwise locations from the onset of separation. For *Re* = 25000 to 55000, *u'* exponentially increases up to x/l = 0.3 followed by a dip near x/l = 0.4, which can be related to the beginning of transition, where the shape factor becomes maximum [24]. After x/l = 0.4, it increases rapidly up to x/l = 0.9, where it becomes maximum and then *u'* decreases slowly depicting the reattachment. However, an exponential growth of *u'* is illustrated from the beginning without any dip for high *Re* = 75000.

Growth rate d(log$u$*)/dx* (u* being u'_{max}/U and x* is x/l) is about 3 till x/l=0.4 for *Re* 25000 to 55000, whereas, for 75000 it is 2.1. In the second-half of the bubble, it increased rapidly and the values are 3.5, 5.4, 7 and 6.5 for *Re* = 25000, 35000, 55000 and 75000 respectively. Thus, development of three-dimensional motions and non-linear interactions of perturbations resulting to breakdown occur in the second-half of the bubble. The growth rate of *u'* drops down to 1.6 to 1.0 with *Re* near the reattachment. Spalart and Strelets [13] did DNS

of separation bubble on a flat plate, where he observed a growth rate of 1-4 in the transition region that drops downs to 2. In the present study, the values of growth rate in the second-half of the bubble is more as compared to the literature pertaining to the separation bubble forming on a flat plate, may be the characteristics of the leading edge flow. It should be noted that the values of *u'* reaches to a maximum of about 22% near reattachment and then approaches to a value around 15% far downstream illustrating a slow relaxation for *Re* up to 55000, whereas, it reaches a maximum level of 15% and then stays around 10% in the downstream for *Re* = 75000.

PRIMARY INSTABILITY

Figure 5 depicts that the velocity profiles have an inflexion point near separation, which is known for the necessary and sufficient condition for flow to be unstable via inviscid instability. However, to illustrate further, the instability mechanism of separated shear layer can be examined in detail. Let us consider two uniform incompressible inviscid fluids of different densities ρ_1 and ρ_2 with velocities U_1, and U_2 be separated by a horizontal boundary. Following the work of Chandrasekhar [25], for a given difference in velocity U_2 - U_1, the K-H instability occurs for all the wave number greater than a critical value irrespective of the velocity difference. K-H instability may occur due to the sharp discontinuities in U or ρ. To clarify this, Chandrasekhar [25] assumed the case of continuous variation of U at a certain distribution of ρ characterised by Richardson number. He concluded that the K-H instability occurs for a band of wave lengths for any value of Richardson number. In particular, when the Richardson number is zero, i.e. for constant density the condition for K-H instability is $0 < K\delta < 1.2785$, where, K is the wave number and δ is shear layer thickness.

It has been already stated that the unsteadiness appears near the separation at x/l = 0.2, Fig. 8. The shear layer thickness (δ) at x/l = 0.2 is estimated from hotwire measurements for different *Re* and are tabulated in Table 2. For example, δ is 0.0039 for *Re* = 25000. Therefore, the unsteady region for K is $0 < K < 325.24$, in other words K-H instability will not occur for wave numbers larger than 325.24 or wavelength (λ) smaller than $2\pi/K = 0.0193$. Figure 10 shows the spectra for different *Re*, where the dominant vortex shedding frequency for *Re* = 25000 is 206 *Hz*. The wave speed (C), corresponding to velocity profiles at x/l = 0.2 is 4.639m/s, which is equal to velocity of the critical layer, where the second derivative of streamwise velocity along wall normal is zero that occurs roughly at 0.043*l*. Therefore, the maximum wave number $K_{max} = 2\pi f/C$ is 279.012 and the corresponding wave length is 0.02252 satisfying the K-H instability criterion for *Re* = 25000. The validity of K-H instability criterion is observed for all other *Re* and are presented in Table 2. Thus, it can be concluded that the transition process is mainly dominated by K-H instability for the range of *Re* considered here.

INTEGRAL PARAMETERS

The variations of integral parameter such as displacement thickness (δ^*), momentum thickness (θ) and shape factor ($H = \delta^*/\theta$) are important to understand the characteristics of shear layer and are presented in Fig. 12. δ^* becomes maximum near x/l = 0.5 and decreases thereafter, whereas, θ increases rapidly in the second-half illustrating augmentation of turbulence and becomes maximum near the reattachment. This results in maximum value of H near the middle (x/l = 0.4 to 0.5) of the bubble for all *Re* indicating beginning of transition [24]. The maximum value of H is around 7.6 for low *Re*, and it being 5.3 for high *Re*. Furthermore, near reattachment, H is around 2.4 to 1.4 as *Re* increases. H approaches to 1.3 indicating a canonical layer far downstream.

The separation criterion $m = \frac{\theta_s^2}{\nu}\left(\frac{du_e}{dx}\right)_s$ (based on the flow condition at separation) evaluated in the present study is presented in Table 3, where the values lie in the range -0.10 to -0.072 as *Re* increases. It should be noted that velocity gradient in the streamwise direction is estimated from the surface pressure measurements. Curle and Skan [26] found m to be $-0.171 < m < -0.068$, whereas, Thwaites [27] suggested value of m as -0.08. Thus, m obtained are within the limit.

Another important integral parameter is the Horton's criteria at reattachment which is defined as $\Lambda_R = \left(\frac{\theta}{u_e}\frac{du_e}{dx}\right)_R$. The suggested value of Λ_R is -0.0082 [1], which was later modified to -0.0059 [28]. In the present experiment, the estimated values of Λ_R lie in the range -0.006 to -0.001 as *Re* increases. Low value of Λ_R particularly at high *Re* may be the characteristics of

Table 2. K-H Instability criterion at x/l = 0.2

Re	$\delta\times10^3$	Limits		f (*Hz*)	C (m/s)	Predicted limits	
		K_{min}	λ			K_{max}	λ
25000	3.931	325.24	0.01932	206	4.639	279.012	0.02252
35000	3.215	397.67	0.01579	405	7.046	361.154	0.01739
55000	2.206	579.5	0.0108	813	8.815	579.5	0.0108
75000	1.478	865.02	0.00726	2090	16.2	810.608	0.00775

Table 3. Variation of Integral parameters with *Re*

Re	Re_{lt}	$Re_{\theta s}$	*m*	Λ_R	$400\ Re_{\theta s}^{0.7}$
25000	14332	82.8	-0.0997	-0.0061	8804
35000	18819	94.1	-0.0945	-0.0026	9625
55000	27612	106.1	-0.0790	-0.0026	10472
75000	26031	120.1	-0.0718	-0.0011	11421

leading-edge induced separated layer. It should be noted here that Horton's or Thwaites criterion is derived neglecting effects of surface curvature. Furthermore, these criteria illustrate that separation occurs in the region of strong adverse pressure gradients, whereas, the reattachment happens before the end of the adverse pressure gradient

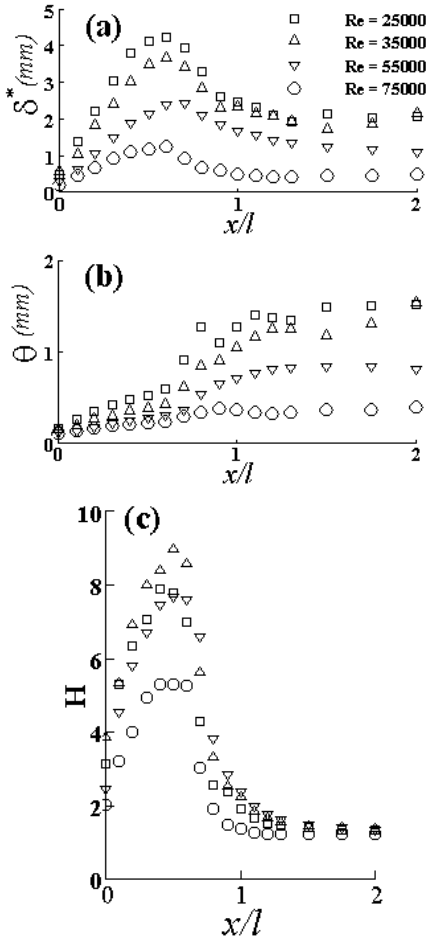

Figure 12 Boundary layer integral parameters: variation of (a) displacement thickness, (b) momentum thickness and (c) shape factor.

RELAXATION OF BOUNDARY LAYER

The time-averaged velocity profiles at different streamwise locations after reattachment obtained from measurements are compared with the log-law, which can explain the relaxation of boundary layer. Figure 13 illustrates that the velocity profile downstream of reattachment is initially very different from equilibrium turbulent boundary layer. It takes about five bubble lengths (*x/l* = 5) to approach to the log-law illustrating relatively slow relaxation for *Re* = 25000, whereas, the velocity profiles approaches to a canonical layer at *x/l* = 3 for *Re* = 75000. Alam and Sandham [14] suggested that the separated layer takes about seven bubble length to attain equilibrium through DNS on a flat plate where, the flow conditions are different.

Variation of Clauser parameter, defined as $G = \frac{H-1}{H}\sqrt{\frac{2}{C_f}}$ is a measure of departure of boundary layer from equilibrium condition. A flat plate boundary layer with zero pressure gradient shows *G* = 6.8 at equilibrium. In the present study, *G* in the immediate vicinity of reattachment is very high attributing to non-equilibrium layer and then decreases monotonically downstream to 6.8 near *x/l* = 3 and then remains constant for *Re* 25000 to 55000, whereas, it decreases to a minimum value of 5.2 at *x/l* = 1.5 and then increases to 6.8 near *x/l* = 3 (figure is not provided because of space). It should be noted that C_f after reattachment is estimated from the measured value of shape factor following the correlation given by Ludwieg-Tillmann [29].

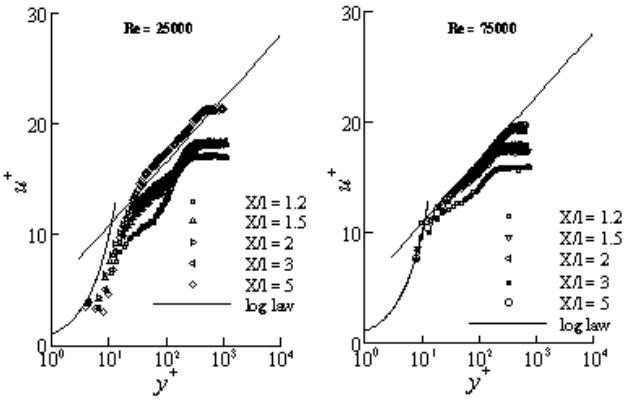

Figure 13 Redevelopment of reattached boundary.

CONCLUSIONS

Experiments are carried out in a low speed wind tunnel to study the transition of a laminar separated layer over a semi-circular leading edge for varying *Re* in the range of 25000 to 75000. The time-averaged velocity and r.m.s quantities are obtained through hotwire probe,

whereas, the instantaneous flow field are measured by PIV. The onset of separation and reattachment points are found with pressure measurements and are also supported by flow visualization. The velocity fluctuations illustrates that the separated shear layer is laminar up to 20% of separation length and then the perturbations grow in the outer layer, which become significant in the second half of the bubble developing three-dimensional motions and breakdown.

The mean bubble length and height decreases with increase in *Re*. There is a significant outer layer activity near the reattachment, which decreases and shifts toward wall with *Re*. Thus, in the vicinity of reattachment and even downstream, the turbulence intensity is high for larger bubble, however, growth rate of disturbances decreases. The instability analysis illustrates that, the shear layer is inviscidly unstable via Kelvin-Helmoltz mechanism for all *Re* considered. Flow visualization by PIV also supports that the development of unsteadiness and three-dimensional motions in the later half of the bubble with formation of K-H rolls and shedding of large-scale vortices that keep their identity far downstream. The predominant shedding frequency when normalised with the momentum thickness at separation remains almost constant with change in *Re*. Following reattachment, a turbulent boundary layer is established depicting a relatively slow relaxation for low *Re*.

REFERENCES

[1] Horton. H. P., Laminar Separation Bubbles in Two and Three-Dimensional Incompressible Flow PhD thesis, Department of Aeronautical Engineering, Queen Mary College, University of London. C. P., 1968, No., 1073

[2] Jones, B. M., Stalling. J. R. Aero. Soc.38, 1934, 747–770.

[3] Gaster. M., The Structure and Behaviour of Laminar Separation Bubbles," Aerodynamics Division N.P.L., 1967, Reports and Memoranda No. 3595

[4] Cherry, N. J., Hiller, R., and Latour, M. E. M. P., Unsteady Measurements in a Separated and Reattaching Flow, J . Fluid Mech. Vol. 144, 1984, pp. 13-46

[5] Kiya, M., and Sasaki, K., Structure of a Turbulent Separation Bubble**,** J . Fluid Mech. Vol. 137, 1983, pp. 83-113

[6] Kiya, M., and Sasaki, K., Structure of Large- Structure of Large-Scale Vortices and Unsteady Reverse Flow in the Reattaching Zone of a Turbulent Separation Bubble, J . Fluid Mech. Vol. 154, 1985, pp. 463-491

[7] Watmuff, J.H., Evolution of a Wave Packet into Vortex Loops in a Laminar Separation Bubble, J. Fluid Mech., Vol. 397, 1999, pp. 119-169

[8] Lang, M., Rist, U., and Wagner, S., Investigations on Controlled Transition Development in a Laminar Separation Bubble by means of LDA and PIV, Experiments in Fluids, Vol. 36, 2004, pp. 43–529

[9] Marxen, O., Lang, M., Rist, U., and Wagner, S., A Combined Experimental/Numerical Study of Unsteady Phenomena in a Laminar Separation Bubble, Flow, Turbulence and Combustion, Vol**.** 71, 2003, pp**.** 133–146

[10] Hain, R., Kahler, C. J., and Radespiel, R., Dynamics of Laminar Separation Bubbles at Low-Reynolds-Number Aerofoils, J. Fluid Mech., Vol. 630, 2009, pp. 129–153.

[11] Ripley. M. D., and Pauley. L. L., The Unsteady Structure of Two Dimensional Steady Laminar Separation, Phys. Fluids A, Vol. 5, 1993, pp. 3099-3106

[12] Muti Lin, J. C., and Pauley, L. L., Low-Reynolds Number Separation on an Airfoil, AIAA J., Vol. 34, 1996, pp. 1570-1577.

[13] Spalart, P. R., and Strelets, M. K., Mechanisms of Transition and Heat Transfer in a Separation Bubble, J. Fluid Mech., Vol. 403, 2000, pp. 329-349

[14] Alam, M., and Sandham, N. D., Direct Numerical Simulation of Short Laminar Separation Bubbles With Turbulent Reattachment, J. Fluid Mech.,Vol 410, 2000, pp. 1–28.

[15] McAuliffe, B.R., and Yaras, M.I., Numerical Study of Instability Mechanisms Leading to Transition in Separation Bubbles, ASME J. Turbomach., Vol. 130, 2008, 021006

[16] Yang, Z. Y., and Voke, P. R., Large-Eddy Simulation of Boundary Layer Separation and Transition at a Change of Surface Curvature, J. Fluid Mech., Vol. 439, 2001, pp. 305–333.

[17] Talan, M., and Hourmouziadis, J., Characteristic Regimes of Transitional Separation Bubbles in Unsteady Flow, Flow, Turbulence and Combustion**,** Vol. 69, 2002, pp. 207–227

[18] McAuliffe, B.R., and Yaras, M.I., Separation Bubble-Transition Measurements on a Low-Re Airfoil Using Particle Image Velocimetry, 2005, ASME Paper No.GT2005-68663

[19] Arena. A. V., and Mueller. T.J., Laminar Separation, Transition and Turbulent Reattachment near the Leading Edge of Airfoils, AIAA Journal, Vol. 18, 1980, Article No. 79-0004R

[20] Roshko. A., Lau. J. K., Prod. Heat Transfer Fluid Mech.," Inst., 18, 1965, 157-167

[21] Pauley, L. L., Moinz. P., and Reynolds**,** W. C., The Structure of Two-Dimensional Separation, J. Fluid Mech., Vol. 220, 1990, pp. 397-411

[22] McAuliffe, B. R., Yaras, M. I., ransition Mechanisms in Separation Bubbles under Low and Elevated Free-stream Turbulence, ASME J. Turbomach., Vol. 132, 2010, pp 0110041 - 011004-10

[23] Na. Y., and Moin. P., Direct Numerical Simulation of a Separated Turbulent Boundary Layer, J. Fluid Mech., Vol. 374, 1998, pp. 379-405.

[24] Ellsworth. R. H., Mueller. T. J., Airfoil Boundary Layer measurements at Low *Re* in an Accelerating Flow from a Nonzero Velocity, Experiments in Fluids, Vol. 11, 1991, pp.368-374.

[25] Chandrasekar, S.,1961, *Hydrodynamic and Hydromagnetic Stability*, Clarendon Press, Oxford.

[26] Curle, N., and Skan, S. W., Approximate methods for predicting separation properties of laminar boundary layers, Aero.Q. Vol. 8, 1957, pp. 257-268.

[27] Thwaites B., Approximate calculation of the laminar boundary layer., Aero. Vol Q. Vol. 14, 1949, pp. 61-85.

[28] Roberts, W. B., Calculation of laminar separation bubbles and their effect on aerofoil performance. AIAA J. Vol 18, 1980, pp. 25-31.

[29] Hinze, J.O., *Turbulence,* McGraw-Hill, New York, 1959.

[30] Sarkar, S., Identification of Flow Structures on a LP Turbine Blade Due to Periodic Passing Wakes, ASME J. Fluids Eng., Vol. 130, 2008, 061103

[31] Sourabh S. Diwan, and Ramesh, O. N., On the Origin of the Inflectional Instability of a Laminar Separation Bubble, J. Fluid Mech., Vol. 629, 2009, pp. 263–298

[32] Tafti, D. K., and Vanka, S. P., A Three Dimensional Numerical Study of Flow Separation and Reattachment on a Blunt Plate, Phys. Fluids A, Vol. 3, 1991, pp. 1749-1759

[33] Yavuzkurt,S., A Guide to Uncertainity Analysis of Hot-Wire Data, ASME J. Fluids Eng., Vol. 106, 1984, pp. 181-186